

---

# Metric Learning-enhanced Optimal Transport for Biochemical Regression Domain Adaptation

---

Fang Wu<sup>\*1</sup> Nicolas Courty<sup>\*2</sup> Zhang Qiang<sup>\*3</sup> Jiyu Cui<sup>4</sup> Ziqing Li<sup>5</sup>

## Abstract

Generalizing knowledge beyond source domains is a crucial prerequisite for many biomedical applications such as drug design and molecular property prediction. To meet this challenge, researchers have used optimal transport (OT) to perform representation alignment between the source and target domains. Yet existing OT algorithms are mainly designed for classification tasks. Accordingly, we consider regression tasks in the unsupervised and semi-supervised settings in this paper. To exploit continuous labels, we propose novel metrics to measure domain distances and introduce a posterior variance regularizer on the transport plan. Further, while computationally appealing, OT suffers from ambiguous decision boundaries and biased local data distributions brought by the mini-batch training. To address those issues, we propose to couple OT with metric learning to yield more robust boundaries and reduce bias. Specifically, we present a dynamic hierarchical triplet loss to describe the global data distribution, where the cluster centroids are progressively adjusted among consecutive iterations. We evaluate our method on both unsupervised and semi-supervised learning tasks in biochemistry. Experiments show the proposed method significantly outperforms state-of-the-art baselines across various benchmark datasets of small molecules and material crystals.

## 1. Introduction

Domain adaptation (DA) is critical to ensuring the reliability and safety of machine learning systems (Yang et al., 2021), since the data used for learning and inference are not likely to follow the same distribution. Discrepancies or shifts in data distributions originate from several reasons and are application-dependent (Jhuo et al., 2012).

In the area of biochemistry, shift always occurs when global environmental states such as temperature and pressure (Chen et al., 2019a) change. Additionally, learning from one category of molecules and trying to deploy an application targeted to a wide range of other groups may also be hindered by different distributions of their 3D constructions and atom compositions (Townshend et al., 2020). Besides, the shift can also be observed between simulated data and experimental data (Chen et al., 2021) or among different experimental data due to the batch effect (Leek et al., 2010).

For the above-mentioned reasons, a trustworthy biochemical deep learning system should not only produce accurate predictions on the known compounds, but possess ability to transfer knowledge across domains (Yang et al., 2021). This adaptation endows biochemists with the power to find new potential materials and drugs (Han et al., 2021), and the process of scientific research can be potentially accelerated.

Currently, most DA papers concentrate on the classification settings (Hsu et al., 2020; Zhang et al., 2020; Zhou et al., 2020). But the majority of essential biochemical problems are regression ones, including property prediction (Ramakrishnan et al., 2014; Wu et al., 2018), 3D structure prediction (Jumper et al., 2021), molecular generation (Madani et al., 2020), and binding affinity prediction (Wang et al., 2005). Only few techniques are universally applicable for regression tasks (Arjovsky et al., 2019; Li et al., 2021), but they fail to tackle them in the biochemical background. Jin et al. (2020) improve IRM (Arjovsky et al., 2019) with predictive regret to generalize to new scaffolds or protein families, but leave semi-supervised DA (Semi-DA) out of consideration. More crucially, his data splits based on heavy atom numbers and scaffold molecule weights fail to be realistic and are less likely to represent real-world biomedical applications. Apart from that, Chen et al. (2021) merge

---

<sup>1</sup>Columbia University, New York, USA <sup>2</sup>Southern Brittany University, Lorient, France <sup>3</sup>Department of Computer Science and Technology, Zhejiang University, Hangzhou, China <sup>4</sup>Department of Chemical Engineering, Zhejiang University, Hangzhou, China <sup>5</sup>Department of Engineering, Westlake University, Hangzhou, China. Correspondence to: Ziqing Li <Stan.ZQ.Li@westlake.edu.cn>.

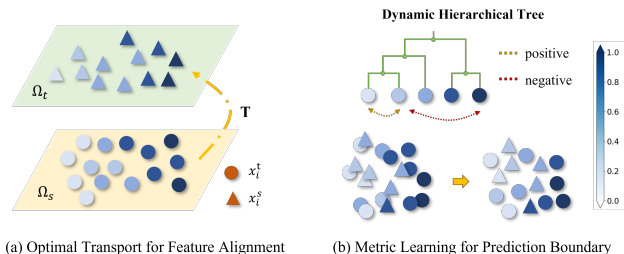


Figure 1. The architecture of our proposed BROT. Sub-figure (a) depicts the OT process to align features from different domains. Sub-figure (b) shows that the metric learning aims to seek better decision boundaries with a dynamic hierarchical tree. The darkness of blue colors reflects the magnitude of molecular properties.

multiple material datasets by introducing an additional state variable to indicate the fidelity of each dataset. Though this framework is applicable across both ordered and disordered materials, it requires a full access to labeled data of multiple domains.

Recently, optimal transport (OT) has been proven as a promising tool to perform DA tasks (Sun et al., 2017; Damodaran et al., 2018) including heterogeneous DA (Yan et al., 2018) and multi-source DA (Nguyen et al., 2021). It learns the transformation across domains under a minimal cost with theoretical guarantees (Seguy et al., 2017; Redko et al., 2017). However, existing OT methods are primarily constrained by two bottlenecks for our biochemical DA problems. First, the exploitation of label information in current OT methodologies are mainly designed for class labels. For example, OTDA (Courty et al., 2016) resorts to a regularization preventing the transport plan from moving two source points of different classes onto the same target point. But it brings unique challenges to regularize the transport strategy according to the continuous molecular properties. JDOT (Courty et al., 2017) strives to minimize the OT loss between the joint source distribution and an estimated target distribution for unsupervised DA (UDA), but neglects the label information in the source domain to constrain the OT plan. Second, OT for DA is on the basis of the mini-batch training manner and the Euclidean metric. The sampled instances within mini-batches are unable to fully reflect the real distribution. Thus, the estimated transport plan is biased (Li et al., 2020). While a few studies have been introduced to either learn a better metric (Zhou et al., 2020; Dhouib et al., 2020; Kerdoncuff et al., 2021) or reduce the bias brought by mini-batches (Li et al., 2020; Fatras et al., 2021a), none of them succeed in realizing those two objectives simultaneously.

To address aforementioned issues, we propose a novel OT method specifically designed for Biochemical Regression DA problems and name it BROT (see Figure 1). In this work, we analyze two variants of DA, UDA and Semi-

DA. First, we design different metrics to measure distances across domains for these two variants, and impose a posterior variance regularizer on the transport plan to fully employ the regression label information in the source domain. Second, in order to seek a better OT metric, we couple OT with a dynamic hierarchical triplet loss. This helps achieve a more distinguishable feature space and avoid ambiguous decision boundaries. More importantly, this loss is dynamically calculated to overcome the flaw of OT’s mini-batch training. It explores the data distribution obtained in the previous iteration to guide the differentiation of samples in the current stage, so OT can jump out of biased local data distributions and align domains from a global perspective. Our contributions are summarized as follow:

- To the best of our knowledge, we are the foremost to propose a novel OT method for both UDA and Semi-DA regression problems in the biomedical field.
- We improve OT with a dynamic hierarchical triplet loss to achieve robust decision boundaries and decrease the bias caused by the mini-batch training.
- Our experiments indicate convincing declines of DA errors and we outperform previous state-of-the-art baselines on real-world biochemical datasets.

## 2. Preliminary

### 2.1. Domain Adaptation Problem Statement

Throughout the paper, we consider a biochemical regression task  $g : \mathcal{X} \rightarrow \mathcal{Y} \subseteq \mathbb{R}$ , where  $\mathbf{x} \in \mathcal{X}$  can be any small molecules, crystals, or proteins, and  $\mathbf{y} \in \mathcal{Y}$  represents a sort of physical or chemical property such as hydration free energy (Mobley & Guthrie, 2014) and binding affinity (Wang et al., 2005). Let  $\mathcal{E}^t$  be the target domain set that we want to adapt to, and  $\mathcal{E}^s$  be the source domain set.  $(\mathbf{x}_i^e, y_i^e)$  and  $\mathcal{D}^e$  denote an input-label pair and a dataset drawn from the data distribution of some domain  $e \in \mathcal{E}^s \cup \mathcal{E}^t$ , respectively.

The goal of DA is to seek a regressor  $g^*$  that minimizes the worst-domain loss on  $\mathcal{E}^t$ :

$$g^* = \operatorname{argmin}_{g \in \mathcal{G}} \mathcal{L}^{\mathcal{E}}(\mathcal{E}^t, g) \quad (1)$$

$$\mathcal{L}^{\mathcal{E}}(\mathcal{E}, g) \triangleq \max_{e \in \mathcal{E}} \mathbb{E}[\ell(g(\mathbf{x}_i^e), y_i^e)] \quad (2)$$

where  $\mathcal{G} : \mathcal{X} \rightarrow \mathbb{R}$  is the Hypothesis space and  $\ell$  is the loss function. Furthermore, the problem is simplified in our setting, where we only consider a single source domain  $s$  and a single target domain  $t$  instead of two domain sets. Practically, our aim is to minimize the error of a dataset in the target domain as  $\operatorname{err}_{\text{DA}}(g) = \mathcal{L}^{\mathcal{D}}(\mathcal{D}^t, g)$ , where  $\mathcal{L}^{\mathcal{D}}$  corresponds to the total loss of  $g$  on a given dataset  $\mathcal{D}$ .

Similar to previous works (Arjovsky et al., 2019; Creager et al., 2020; Jin et al., 2020; Krueger et al., 2021; Ye et al.,

2021),  $g$  is assumed to be decomposed into  $f \circ h$ , where  $f : \mathcal{X} \rightarrow \mathbb{R}^d$  is the feature extractor that maps input into the feature space  $\mathcal{H}$  and  $h : \mathbb{R}^d \rightarrow \mathbb{R}$  is the predictor. Additionally, DA strategies can be roughly divided into two families as Semi-DA (Kulis et al., 2011) and UDA (Gopalan et al., 2011; Gong et al., 2012), depending on the presence of few labels in the target domain set  $\mathcal{E}^t$ .

Typically, one assumes the existence of two distinct joint probability distributions  $\mathbb{P}_s(\mathbf{x}^s, \mathbf{y}^s)$  and  $\mathbb{P}_t(\mathbf{x}^t, \mathbf{y}^t)$  defined over  $\mathcal{X} \times \mathcal{Y}$  and related to the source and target domains respectively. We denote them as  $\mathcal{P}^s$  and  $\mathcal{P}^t$  for sake of simplicity. Appendix A.1 lists common assumptions made by most DA methods, including property imbalance and covariate shift. We also provide methods to measure the variation and informativeness of  $f$  in Appendix A.2.

## 2.2. Domain Adaptation in Biochemistry

DA has been intensively researched since its first emergence (Hendrycks & Gimpel, 2016). In classification tasks, people regard data with class labels unseen in the source training set  $y_i \notin \mathcal{Y}^s \subseteq \mathbb{Z}^+$  as the domain with a semantic shift (SS). These categorical labels explicitly indicate their corresponding classes. In contrast, data represented in different forms are regarded as DA with a non-semantic shift (NS). For instance, pictures can be shown in cartoon, sketch, real, etc (Hsu et al., 2020).

However, it is not straightforward to conceptualize the shift types for regression tasks in the biochemical field. To fill in this gap, we identify molecules with properties that are not in the range of the training set  $y_i \notin \mathcal{Y}^s \subseteq \mathbb{R}$  as SS (see Figure 2). To be specific, the space of the property values in two different domains  $s$  and  $t$  with SS ought to be different as  $\mathcal{Y}^s - \mathcal{Y}^t \neq \emptyset$ . Besides that, a molecule is identified as NS if it is drawn from an unseen kind. For example, macromolecules such as polyphenols and nucleic acids can be treated as NS to small molecules like heteronuclear diatomic molecules. Four basic types of crystals containing covalent, ionic, metallic, and molecular crystals, can also be considered as NS to each other. Moreover, NS exists between the simulated data and the experimental data.

## 3. Optimal Transport for Regressions

### 3.1. Unsupervised Domain Adaptation

UDA is common in biochemistry. The ground truth of property distributions in the target domain  $\mathbb{P}_t(\mathbf{y}^t)$  is inaccessible and labels are only available in the source domain. Generally, UDA is correlated with SS. For instance, an adaptation from drugs with low Topological Polar Surface Area (TPSA) to those with high TPSA (Ertl et al., 2000).

The priority in UDA is to decide a metric to measure the

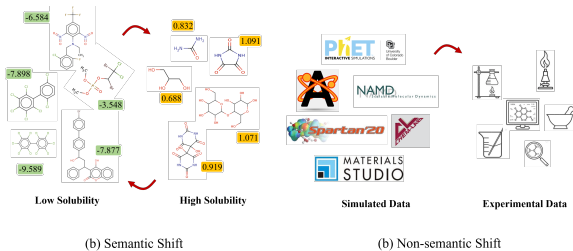


Figure 2. Examples of the two sorts of distribution shifts in biochemistry. In sub-figure (a), molecules with different ranges of properties are viewed as semantic shift. The numbers in green and orange represent the magnitude of compounds’ solubility. In sub-figure (b), simulated data and experimental data are from two different domains with non-semantic shift.

distance between  $\mathbf{x}^s$  and  $\mathbf{x}^t$  on the ground space  $\mathcal{Z} = \mathcal{X}$ . In most applications, the metric in the feature space,  $d_{\mathcal{H}}$ , is readily available and the Euclidean distance is a popular option (Courty et al., 2016). Consequently, the distance between two molecules  $d_{\mathcal{Z}}^f : \mathcal{X} \times \mathcal{X} \rightarrow \mathbb{R}^+$  is defined as:

$$d_{\mathcal{Z}}^f(\mathbf{x}_i^s, \mathbf{x}_j^t) = d_{\mathcal{H}}(f(\mathbf{x}_i^s), f(\mathbf{x}_j^t)) \quad (3)$$

### 3.2. Semi-supervised Domain Adaptation

Semi-DA is a more realistic setting, where learners have access to a small amount of labeled data but no unlabeled data from the target domain. It usually occurs with NS. A typical example is the adaptation from a large amount of simulated data to a small quantity of real-world experimental data (Chen et al., 2021), which is prohibitively labor-expensive, error-prone, and time-consuming to be collected (Le et al., 2021).

First, we define a metric to measure the distance between  $(\mathbf{x}^s, \mathbf{y}^s)$  and  $(\mathbf{x}^t, \mathbf{y}^t)$  on the ground space  $\mathcal{Z} = \mathcal{X} \times \mathcal{Y}$ . A forthright way is via individual metrics in  $\mathcal{H}$  and  $\mathcal{Y}$ , and sum them together like JDOT (Courty et al., 2017). Then for  $p \geq 1$ , a naive solution  $d_{\mathcal{Z}}^f : (\mathcal{X} \times \mathcal{Y})^2 \rightarrow \mathbb{R}^+$  is:

$$d_{\mathcal{Z}}^f((\mathbf{x}_i^s, y_i^s), (\mathbf{x}_j^t, y_j^t)) = d_{\mathcal{H}}(f(\mathbf{x}_i^s), f(\mathbf{x}_j^t))^p + \epsilon d_{\mathcal{Y}}(y_i^s, y_j^t)^p \quad (4)$$

where  $\epsilon$  is a hyper-parameter to balance distances in two spaces  $\mathcal{H}$  and  $\mathcal{Y}$ , and  $d_{\mathcal{Y}}$  is the metric in  $\mathcal{Y}$ . Similarly, we can exploit the Euclidean distance as  $d_{\mathcal{H}}$ . As for  $d_{\mathcal{Y}}$ , it is no longer an obstacle to compute it as in the discrete label space (Alvarez-Melis & Fusi, 2020), since the original metric in  $\mathcal{Y}$  can be directly utilized there.

Although attractive for its simplicity, this addition operation ignores the mutual relationship between  $\mathcal{H}$  and  $\mathcal{Y}$ . Besides, Equation 4 is sensitive to  $\epsilon$ , and an instance study illustrates its unbalanced attention to  $d_{\mathcal{H}}$  and  $d_{\mathcal{Y}}$  as shown in Appendix B.1. Intuitively, two molecules with mismatched properties are supposed to behave significantly different in the feature space, and vice versa.

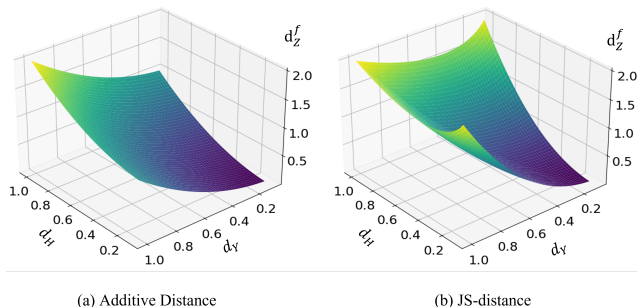


Figure 3. The cost functions of different metrics in Semi-DA. The  $x$ - and  $y$ -axis correspond to the distances in  $\mathcal{H}$  and  $\mathcal{Y}$ , and the darkness of color reflects the magnitude of  $d_{\mathcal{Z}}^f$ .

Motivated by this analysis, we take the form of a Jensen–Shannon (JS) divergence (Lin, 1991) to constrain the discrepancy between each feature-label pair as:

$$d_{\mathcal{Z}}^f((\mathbf{x}_i^s, y_i^s), (\mathbf{x}_j^t, y_j^t)) = d'_{\mathcal{H}}{}^p + \epsilon d'_{\mathcal{Y}}{}^p + \kappa \left( \left| d'_{\mathcal{Y}}{}^p \log \left( \frac{d'_{\mathcal{H}}{}^p}{d'_{\mathcal{Y}}{}^p + \zeta} \right) \right| + \left| d'_{\mathcal{H}}{}^p \log \left( \frac{d'_{\mathcal{Y}}{}^p}{d'_{\mathcal{H}}{}^p + \zeta} \right) \right| \right) \quad (5)$$

where  $|\cdot|$  ensures non-negativeness, and  $\kappa$  is a hyperparameter.  $d'_{\mathcal{H}}$  is the normalized value of  $d_{\mathcal{H}}$  as  $d'_{\mathcal{H}}(f(\mathbf{x}_i^s), f(\mathbf{x}_j^t)) = \frac{d_{\mathcal{H}}(f(\mathbf{x}_i^s), f(\mathbf{x}_j^t))}{d_{\mathcal{H}_{max}}}$ , where  $d_{\mathcal{H}_{max}}$  is the maximum distance of all source-target pairs in the feature space, and  $d'_{\mathcal{Y}}$  is adjusted in the same way.  $d'_{\mathcal{H}}$  and  $d'_{\mathcal{Y}}$  are therefore between 0 and 1.  $\zeta > 0$  is added to prevent the zero division error.

Particularly, Equation 5 depends on two components: the addition of  $d'_{\mathcal{Y}}$  and  $d'_{\mathcal{H}}$  accompanied by the JS term. The former requires the source and target samples to carry similar properties and features, while the latter imposes a strong penalty over the disagreement of  $d'_{\mathcal{H}}$  and  $d'_{\mathcal{Y}}$  (see Figure 3). Thus, with this JS-distance metric,  $d_{\mathcal{Z}}^f$  takes into account the magnitude of properties and features as well as the joint connection between two metrics synchronically.

### 3.3. Mini-batch Optimal Transport for DA

Equipped with this novel cost function in  $\mathcal{Z}$ , our goal is to minimize a geometric notion of distance between  $\mathcal{P}^s$  and  $\mathcal{P}^t$ . Following Courty et al. (2016; 2017), we rely on a minimization of the Kantorovich OT problem (Peyré et al., 2019) between joint laws  $\mathcal{P}^s$  and  $\mathcal{P}^t$ , and with respect to the target function  $f$ . As the full OT problem is untractable for large distributions, we rely on mini-batch computation, which has shown recently to be accommodate well with a stochastic optimization over  $f$  (Fratras et al., 2021b).

We assume a training batch  $\mathcal{B} = \mathcal{B}^s \cup \mathcal{B}^t$  contains a source batch  $\mathcal{B}^s = \{(\mathbf{x}_i^s, y_i^s)\}_{i=1}^b$  and a target batch  $\mathcal{B}^t = \{(\mathbf{x}_i^t, y_i^t)\}_{i=1}^b$ . Explicitly, for UDA  $\mathcal{B}^t$  comes from all unlabeled

data attainable in the target domain, while for Semi-DA it is drawn only from labeled data. Here  $b$  is the mini-batch size. More formally, our objective function is:

$$d_{\text{OT}}^f(\mathcal{D}^s, \mathcal{D}^t) = \mathbb{E} \left[ \min_{\mathbf{T} \in \Pi(\mathcal{B}^s, \mathcal{B}^t)} \langle \mathbf{T}, \mathbf{D}_{\mathcal{Z}}^f \rangle \right] \quad (6)$$

where  $\mathbf{D}_{\mathcal{Z}}^f$  is the matrix of all pairwise distances between elements of the source and target batches, and  $\mathbb{E}$  takes the expectation with respect to the randomly sampled mini-batches drawn from both domains. This optimization is conducted over  $\Pi(\cdot, \cdot)$ , which is the set of all matrices with prescribed uniform marginals defined as:

$$\Pi(\mathcal{B}^s, \mathcal{B}^t) = \{ \mathbf{T} \in \mathbb{R}_+^{b \times b} \mid \mathbf{T} \mathbf{1}_b = \mathbf{u}_b, \mathbf{T}^\top \mathbf{1}_b = \mathbf{u}_b \} \quad (7)$$

where  $\mathbf{u}_b$  is the uniform distribution of size  $b$ .

### 3.4. Regularization by Variance Reduction

Though appealing, OT suffers from several defects such as bad sample complexity (Weed & Bach, 2019), with an exponential dependence in the data dimension, and does not, in its initial formulation, leverage on all DA specificities. A classical way for better conditioning the problem is to add regularization terms. Cuturi (2013) smooth  $\mathbf{T}$  by a penalty on its entropy, and has the twofold advantage of making the problem strongly convex while allowing for faster computations with the celebrated Sinkhorn algorithm (Peyré et al., 2019), with a near linear time complexity (Altschuler et al., 2017). In a context of classification DA tasks, class-based regularization (Courty et al., 2016) tremendously improves the performance. However, to the best of our knowledge, no such regularization exists in a regression context. We bridge this gap by imposing a similar type of regularization which minimizes, for a given sample in the target domain, the variance of the associated properties in the source domain.

We start by defining a posterior probability distribution of the property for the  $j^{\text{th}}$  target sample and noting  $Y_j$  the corresponding random variable.  $Y_j$  takes  $\mathbf{y}^s$  as possible values with probabilities given by the  $j^{\text{th}}$  column of the coupling matrix  $\mathbf{T}$  (noted  $\mathbf{t}_j$ ), divided by the probability of having this sample. As batches are uniform distributions of samples, this vector of probability is simply  $b\mathbf{t}_j$ . Intuitively, we seek to minimize the variance of the transported properties for a given sample. Therefore, for a given target sample  $j$ , the regularizer  $\Omega_p^{\mathbf{y}^s}$ , being a function of  $\mathbf{t}_j$ , is defined as:

$$\Omega_p^{\mathbf{y}^s}(\mathbf{t}_j) = \text{var}_{\mathbf{t}_j}(Y_j) = b \sum_{i=1}^b T_{ij} \left( y_i^s - \sum_{l=1}^b b T_{lj} \cdot y_l^s \right)^2 \quad (8)$$

where  $\text{var}$  is the variance. A small  $\Omega_p^{\mathbf{y}^s}$  guarantees that the  $j^{\text{th}}$  target sample receives masses only from source samples with close properties, and therefore induces a desired representation for them. We finally note  $\Omega_p^{\mathbf{y}^s}(\mathbf{T}) = \sum_j \Omega_p^{\mathbf{y}^s}(\mathbf{t}_j)$  the total regularization over every samples of the target.

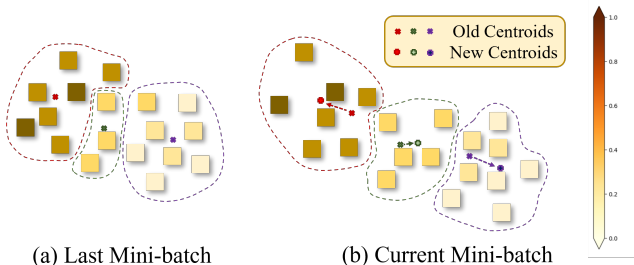


Figure 4. **The dynamic cluster centroids in our triplet loss.** The centroids in the last mini-batch are used to help cluster molecules in the current mini-batch, and then are updated afterwards. The darker is the orange, the higher is the molecular properties.

The final formulation of our problem, combining both entropy and posterior variance regularization, is:

$$d_{\text{OT}}^f(\mathcal{D}^s, \mathcal{D}^t) = \mathbb{E} \left[ \min_{\mathbf{T} \in \Pi(\mathcal{B}^s, \mathcal{B}^t)} \langle \mathbf{T}, \mathbf{D}_{\mathcal{Z}}^f \rangle + \lambda_1 \Omega_e(\mathbf{T}) + \lambda_2 \Omega_p^{y^s}(\mathbf{T}) \right] \quad (9)$$

where  $\Omega_e(\mathbf{T}) = \sum_{i,j} T_{ij} \log T_{ij}$  is the entropy constraint.  $\lambda_1 > 0$  and  $\lambda_2 > 0$  are hyperparameters controlling the importance of different regularization terms. As  $\Omega_p^{y^s}(\mathbf{T})$  is concave in  $\mathbf{T}$  (see Appendix C.1), the corresponding optimization problem is a difference of convex program (DC). Given  $f$ , this problem can be solved thanks to a generalized conditional gradient approach (Rakotomamonjy et al., 2015; Courty et al., 2016), and we use the corresponding POT implementation (Flamary et al., 2021). More details on the optimization procedure are given in Appendix C.2.

Used in the final loss of our problem, we need to compute  $\min_f d_{\text{OT}}^f(\mathcal{D}^s, \mathcal{D}^t)$ , which consists in two nested optimization problems. In order to compute the gradient wrt.  $f$ , we use the Envelope theorem (Bonnans & Shapiro, 1998): since  $f$  is only involved in the cost matrix  $\mathbf{D}_{\mathcal{Z}}^f$ , we first compute for given mini-batches an optimal coupling  $\mathbf{T}^*$  (by solving problem 9), and consider it fixed to backpropagate through the loss  $\langle \mathbf{T}^*, \mathbf{D}_{\mathcal{Z}}^f \rangle$ . This strategy is a fairly common practice when using OT in a context of deep learning (Damodaran et al., 2018; Fatras et al., 2021a).

## 4. Metric Learning with Dynamic Triplet Loss

### 4.1. Metric Learning for DA

Domain alignment via OT is not sufficient for DA due to several reasons. Most importantly, existing OT distances including Euclidean and Wasserstein used in the cost matrix may be a sub-optimal metric (Kerdoncuff et al., 2021), leading to ambiguous decision boundaries (Dou et al., 2019; Zhou et al., 2020). When predicting on the target domain,

the learner tends to suffer from them. To overcome that issue, we employ the metric learning to help separate the instances and promote unequivocal prediction boundaries for superior adaptation.

The goal of metric learning is to learn a distance function under semantic constraints, which brings closer samples of the same class while pushes away data of different labels (Kulis et al., 2013). However, it requires extra domain knowledge to subtly classify molecules based on their properties.

To this end, we utilize a K-means (Hartigan & Wong, 1979) algorithm to construct a hierarchical class-level tree and encode the global context information, where the hierarchical structure can naturally capture the intrinsic data distribution across domains (Langfelder et al., 2008). In addition, although data structures in the feature space change constantly during the training process, the relative positions of data points are roughly preserved (Ge, 2018). This enables us to take advantage of the local data distribution gained in previous iterations to help cluster molecules in the current iteration. Specifically, we progressively adjust the cluster centroids during each iteration so that the information regarding the global data distribution is revealed (see Figure 4). As a consequence, it is feasible to jump out of local data distributions within mini-batches and consider a global data distribution of multiple domains.

### 4.2. Dynamic Triplet Loss

Our dynamic triplet loss also follows a mini-batch training manner. At the initial step ( $t = 0$ ), we partition all  $2b$  observations within each mini-batch into  $K$  fine-grained clusters through K-means and attain  $K$  corresponding cluster centers  $\mathbf{M}^{(0)} = \{\mathbf{m}^{(0)}\}_{i=1}^K$ . Then we calculate the distance matrix  $\mathbf{D}_{\mathcal{C}} \in \mathbb{R}^{K \times K}$  of those  $K$  clusters, where the distance between the  $p^{\text{th}}$  and the  $q^{\text{th}}$  cluster is defined as:

$$d_{\mathcal{C}}(p, q) = \frac{1}{n_p n_q} \sum_{i \in p, j \in q} d_{\mathcal{Z}}^f((\mathbf{x}_i, y_i), (\mathbf{x}_j, y_j)) \quad (10)$$

where  $n_p$  and  $n_q$  are the numbers of samples belonging to the  $p^{\text{th}}$  and the  $q^{\text{th}}$  cluster. As for UDA,  $d_{\mathcal{C}}$  is calculated based on  $d_{\mathcal{Z}}^f(\mathbf{x}_i, \mathbf{x}_j)$ , and we deemphasize this difference in the rest of this chapter. After that, a hierarchical tree  $\Upsilon^{(0)}$  is created by recursively merging the leaf nodes at different levels according to the distance matrix  $\mathbf{D}_{\mathcal{C}}$  (Moore, 2001).

Next, triplets are constructed as  $\psi = (\mathbf{x}_{\text{anc}}, \mathbf{x}_{\text{pos}}, \mathbf{x}_{\text{neg}})$ , which contains an anchor sample  $x_{\text{anc}}$ , a positive sample  $x_{\text{pos}}$ , and a negative sample  $x_{\text{neg}}$ . Finally, the triplet loss can

be formulated as:

$$\mathcal{L}_m = \frac{1}{|\Psi^{\mathcal{B}}|} \sum_{\psi \in \Psi} \left[ d_{\mathcal{Z}}^f((\mathbf{x}_{\text{anc}}, y_{\text{anc}}), (\mathbf{x}_{\text{pos}}, y_{\text{pos}})) - d_{\mathcal{Z}}^f((\mathbf{x}_{\text{anc}}, y_{\text{anc}}), (\mathbf{x}_{\text{neg}}, y_{\text{neg}})) + \mu \right]_+ \quad (11)$$

where  $[\cdot]_+ = \max(\cdot, 0)$  is the ramp function, and  $\Psi^{\mathcal{B}}$  and  $|\Psi^{\mathcal{B}}|$  are the set and number of all triplets in the mini-batch  $\mathcal{B}$ , respectively.  $d_{\mathcal{Z}}^f((\mathbf{x}_{\text{anc}}, y_{\text{anc}}), (\mathbf{x}_{\text{pos}}, y_{\text{pos}}))$  and  $d_{\mathcal{Z}}^f((\mathbf{x}_{\text{anc}}, y_{\text{anc}}), (\mathbf{x}_{\text{neg}}, y_{\text{neg}}))$  separately calculate the distance of positive pairs and negative pairs.  $\mu$  is a hierarchical violate margin (Ge, 2018), different from the constant margin of the conventional triplet loss. It is computed in accordance to the relationship between the centroid  $\mathbf{m}_{\text{anc}}^{(0)}$  that the anchor belongs to and the centroid  $\mathbf{m}_{\text{neg}}^{(0)}$  that is related to the negative sample, which takes the following form as:

$$\mu = \mu_0 + d_{\Psi}(\mathbf{m}_{\text{anc}}^{(0)}, \mathbf{m}_{\text{neg}}^{(0)}) \quad (12)$$

where  $\mu_0$  is a small constant that encourages molecular clusters to reside further apart from each other than previous iterations.  $d_{\Psi}(p, q)$  is the threshold for merging the  $p^{\text{th}}$  and  $q^{\text{th}}$  cluster into a single node of the next level. It measures the minimal distance between different clusters in the hierarchical tree  $\Upsilon^{(0)}$ .

In the following iterations ( $t > 0$ ), the training proceeds by alternating between the assignment step and the update step. In the assignment step, samples of a new mini-batch are allocated to  $K$  clusters based on their distances to previous centroids  $\mathbf{M}^{(t-1)}$ . The new  $p^{\text{th}}$  cluster  $\mathcal{S}_p^{(t)}$  can be represented as:

$$\left\{ \mathbf{x}_i : d_{\mathcal{Z}}^f((\mathbf{x}_i, y_i), \mathbf{m}_p^{(t-1)}) \leq d_{\mathcal{Z}}^f((\mathbf{x}_i, y_i), \mathbf{m}_q^{(t-1)}), \forall q \right\} \quad (13)$$

In the update step, the centroids  $\mathbf{M}^{(t)}$  are recalculated by aggregating the means of molecules within this mini-batch assigned to each cluster as:

$$\mathbf{M}^{(t)} = \left\{ \mathbf{m}_p^{(t)} = \frac{1}{|\mathcal{S}_p^{(t)}|} \sum_{\mathbf{x}_i \in \mathcal{S}_p^{(t)}} (\mathbf{x}_i, y_i) \right\}_{p=1}^K \quad (14)$$

At the same time, a new hierarchical tree  $\Upsilon^{(t)}$  is reconstructed according to those new clusters. With  $\Upsilon^{(t)}$ , the triplet loss  $\mathcal{L}_m$  within this mini-batch can also be computed by Equation 11. As the training steps proceed,  $\mathbf{M}^{(t)}$  are dynamically adjusted, and therefore the triplet loss  $\mathcal{L}_m$  varies along with the changing structure of  $\Upsilon^{(t)}$ .

Overall, the whole loss function of BROT per mini-batch consists of three parts, namely the regression task loss  $\mathcal{L}_{\text{reg}}$ ,

---

### Algorithm 1 Workflow of BROT

---

**Require:** A source dataset  $D^s$  with  $N_s$  samples and a target dataset  $D^t$  with  $N_t$  samples. A pre-defined number of total clusters  $K$ .

**Ensure:** Model parameters  $\theta_g$ .

$\mathbf{M}^{(0)} \leftarrow \text{K-means}(\mathcal{B}_{(0)}^s, \mathcal{B}_{(0)}^t) \{ \text{initialize centroids} \}$

**for**  $t = 1, \dots, \lceil \frac{N_s}{b} \rceil - 1$  **do**

$\left\{ \mathcal{S}_i^{(t)} \right\}_{i=1}^K \leftarrow \text{cluster } \mathcal{B}_{(t)}^s \text{ and } \mathcal{B}_{(t)}^t \text{ by Equation 13}$

$\mathbf{M}^{(t)} \leftarrow \text{update } \mathbf{M}^{(t-1)} \text{ by Equation 14}$

Construct a hierarchical tree  $\Upsilon^{(t)}$  by Equation 10

Calculate the regression loss  $\mathcal{L}_{\text{reg}}$

Calculate the loss  $\mathcal{L}_m$  by Equation 11

Compute the optimal coupling  $\mathbf{T}^*$  from Equation 9

Compute the total loss  $\mathcal{L}$  by Equation 15

$\theta_g \leftarrow \theta_g - \nabla_{\theta_g} \mathcal{L}$

**end for**

**return**  $\theta_g^*$

---

the OT loss  $\mathcal{L}_{\text{OT}}$ , and the metric learning loss  $\mathcal{L}_{\text{ml}}$ , which can be written as:

$$\mathcal{L} = \mathcal{L}_{\text{reg}} + \alpha \mathcal{L}_{\text{OT}} + \beta \mathcal{L}_{\text{ml}} \quad (15)$$

where  $\alpha$  and  $\beta$  are used to balance the effects of these three loss terms, and  $\mathcal{L}_{\text{OT}}$  represent the transport distance  $d_{\text{OT}}^f(\mathcal{B}^s, \mathcal{B}^t)$ . Notably,  $\mathcal{L}_{\text{reg}}$  contains the loss of labeled data from both the source and target domain for Semi-DA. The complete training process is shown in Algorithm 1, where we omit the loss in the first mini-batch.

## 5. Experiment

To empirically corroborate the effectiveness of BROT, we evaluate it on real-world applications including molecular property prediction and material adsorption prediction under UDA and Semi-DA, and compare it to existing state-of-the-art methods.  $f$  is implemented as the Molformer (Wu et al., 2021) model, a variant of Transformer (Vaswani et al., 2017), and  $h$  is a two-layer multi-layer perceptron (MLP). Descriptions of benchmark datasets, model architectures, baseline methods, hyperparameter, and other training details are discussed in Appendix D.

### 5.1. Baselines

We highlight the best method in bold and underline the second best for clear comparisons. Our baselines for regression DA tasks include: empirical risk minimization (**ERM**) is trained on all available labeled data of source and target domains; domain adversarial training methods including **DANN** (Ganin et al., 2016) and **CDAN** (Long et al., 2017) seek to learn domain-invariant features; **MLDG** (Li et al.,

2018) is a meta-learning method which simulates domain shift by dividing training environments into meta-training and meta-testing; **JDOT** (Courty et al., 2017) is a OT framework for UDA between joint data distributions.

## 5.2. Unsupervised DA Problem

**Dataset.** To verify the efficacy of BROT, we adopt 6 regression datasets from quantum chemistry and physical chemistry. **QM7** (Blum & Reymond, 2009) is a subset of GDB-13, which records the computed atomization energies of stable and synthetically accessible organic molecules. **QM8** (Ramakrishnan et al., 2015) contains computer-generated quantum mechanical properties including electronic spectra and excited state energy of small molecules. **QM9** (Ramakrishnan et al., 2014) is a comprehensive dataset that provides geometric, energetic, electronic and thermodynamic properties for a subset of GDB-17. **ESOL** (Delaney, 2004) is a small dataset documenting the solubility of compounds. **FreeSolv** (Mobley & Guthrie, 2014) provides experimental and calculated hydration free energy of small molecules in water. The calculated values are derived from alchemical free energy calculations using molecular dynamics simulations. **Lipophilicity** (Gaulton et al., 2012) is selected from ChEMBL, which is an important property that affects the molecular membrane permeability and solubility. The data is obtained via octanol/water distribution coefficient experiments.

**Setup.** For datasets of small molecules, prior work measures model adaptation by splitting the dataset via the number of atoms (Chen et al., 2019b; Tsubaki & Mizoguchi, 2020) or molecular weight (Feinberg et al., 2019). Nevertheless, these two splitting methods are inappropriate as test molecules can be much bigger. The major challenge is that standard scaffold split degenerates to random split when most scaffold clusters contain only one molecule (Jin et al., 2020). Therefore, scaffold split fails to be a perfect measure for biomedical DA problems. Jin et al. (2020) introduce a scaffold complexity split based on the number of cycles in molecular graphs. Nonetheless, cycles are merely a sort of motifs in molecules and this split ignores other frequently occurring and expressive substructures such as amino, carboxyl, and Haloalkanes (Zhang et al., 2021).

Given these observations, we split datasets based on the objective property instead of molecular constituents, which accords with SS. There, we consider a low-to-high environment rather than the high-to-low environment, because molecules with high values of desired properties are traditionally what scientists or pharmacists are searching for in drug or material design (Gómez-Bombarelli et al., 2018; Sanchez-Lengeling & Aspuru-Guzik, 2018). Precisely, the training sets contains molecules with the lowest 80% properties, while the remaining molecules that have the 20%

Table 1. Comparison of performance on small molecule datasets (lower means better). Lipo is the abbreviation of Lipophilicity.

Method	QM7	QM8	ESOL	FreeSolv	Lipo
ERM	83.01±1.26	.040±.008	2.02±.014	2.07±.007	1.21±.054
DANN	81.40±2.14	.033±.012	2.09±.023	2.82±.033	1.22±.076
CDAN	82.85±2.28	.038±.014	2.01±.028	2.06±.019	1.21±.053
MLDG	83.07±3.39	.054±.031	2.04±.044	5.96±1.38	1.29±.081
JDOT	81.78±1.47	.029±.005	2.00±.019	1.96±.079	1.32±.125
<b>BROT</b>	<b>80.14±1.85</b>	<b>.023±.008</b>	<b>1.78±.016</b>	<b>1.93±.046</b>	<b>1.15±.091</b>

Table 2. Comparison of MAE on QM9.

Target Unit	$\epsilon_{\text{HOMO}}$ eV	$\epsilon_{\text{LUMO}}$ eV	$\Delta\epsilon$ eV	$\mu$ D	$\alpha$ bohr <sup>3</sup>
ERM	0.794	0.952	1.021	1.769	3.103
DANN	0.440	0.829	1.032	1.548	3.280
CDAN	0.731	0.916	1.020	1.721	3.101
MLDG	1.043	1.003	1.879	2.714	7.986
JDOT	0.790	0.539	0.850	1.643	2.877
<b>BROT</b>	<b>0.405</b>	<b>0.522</b>	<b>0.728</b>	<b>1.426</b>	<b>2.753</b>

highest properties are equally partitioned into the validation and test sets. Notably, since some unknown molecules can have out-of-distribution properties, our split serves as a more realistic evaluation than preceding splitting methods.

**Results and analysis.** Table 1 and 2 document the mean and standard deviation of three repetitions, where we only select five targets in QM9 that do not require thermochemical energy subtractions. BROT surpasses all baselines with significant margins. Particularly, BROT exceeds JDOT, illustrating its validity to discover better decision boundaries and overcome the drawbacks of mini-batch training. Besides, both DANN and CDAN achieve lower error than ERM, which means learning invariant representations can benefit UDA to some extent on the biomedical regression tasks. Remarkably, the improvement brought by BROT over other approaches in QM8 and QM9 is higher than that in ESOL, FreeSolv and Lipo, which have less than 5K samples. This is because large datasets have more mini-batches, so the bias of the local data distribution in mini-batches with respect to the global data distribution is much greater. The dynamic loss empowers BROT to resist this bias. Thus, the advantage of BROT is enhanced when the data size increases.

## 5.3. Semi-supervised DA Problem

**Dataset.** The algorithm for Semi-DA is evaluated on the adsorption material dataset. It consists of crystals from two domains, which are the simulated data and the experimental data. Explicitly, **CoRE-MOF** (Chung et al., 2019) owns over 10K crystal samples and a wide variety of 79 atom classes. It is obtained from the Cambridge Structural Database (Groom et al., 2016) and a Web of Science (Ana-

Table 3. Comparison of RMSE (lower means better),  $R_p$  and  $R_s$  on Exp-MOF with 25% and 50% labeled target data.

Method	25% Labeled Target			50% Labeled Target		
	RMSE	$R_p$	$R_s$	RMSE	$R_p$	$R_s$
ERM	28.51	0.382	0.370	26.37	0.410	0.408
DANN	26.83	0.399	0.401	26.64	0.407	0.392
CDAN	29.44	0.504	0.531	26.82	0.466	0.521
MLDG	<u>23.70</u>	<u>0.543</u>	<u>0.601</u>	<u>20.77</u>	<u>0.629</u>	<u>0.677</u>
BROT	<b>20.45</b>	<b>0.552</b>	<b>0.617</b>	<b>19.42</b>	<b>0.659</b>	<b>0.710</b>

lytics, 2017) search, and is derived through semi-automated reconstruction of disordered structures using a topology-based crystal generator. CoRE-MOF offers 12 chemical properties, such as LFPD, ASA, carbon dioxide adsorption, etc. Nonetheless, most of its materials is unable to be synthesized. Contrarily, **Exp-MOF** contains samples that can be synthesized and are acquired throughout rigorous and high-priced experiments. But due to the expensive costs, its data size is much smaller with only 113 crystals. CoRE-MOF and Exp-MOF share a same target label, the adsorption capability of materials to carbon dioxide. We aspire to adapt our model to forecast that from CoRE-MOF to Exp-MOF.

**Setup.** To meet the setting of Semi-DA, we randomly select a ratio (25% or 50%) of Exp-MOF with labeled target samples for training and use the rest as the test set. There each method is conducted three times due to the small size of Exp-MOF, and we report their mean performance.

**Results and analysis.** Table 3 reports the Root Mean Squared Error (RMSE), the Pearson correlation ( $R_p$ ), and the Spearman correlation ( $R_s$ ) in Table 3 with 25% and 50% labeled target data. The superiority of BROT over baseline methods is supported by its lowest MAE and highest correlations of both Spearman and Pearson. It is worth noting that although MLDG performs poorly in UDA, it beats adversarial methods in Semi-DA, demonstrating the efficacy of meta-learning when the size of the target dataset is small.

#### 5.4. Ablation Study and Feature Visualization

We examine effects of each component in BROT. Table 5 compares the performance of ERM, OT without regularization, OT with the entropy constraint, OT with all regularization, triplet loss only, and BROT. It demonstrates that the posterior variance regularization contributes to a substantial decrease of the adaptation error. Moreover, OT coupled with the dynamic hierarchical triplet loss produces a better performance than the adoption of either of them. We also provide the comparison results between two different metric designs for Semi-DA in Appendix D.4. The experiment results strongly backup our statement that the JS-distance metric outweighs the additive distance metric. Besides, it is

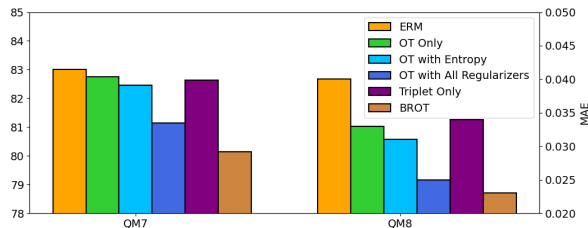


Figure 5. Ablation studies in QM7 and QM8. The Y-axis are of different scales.

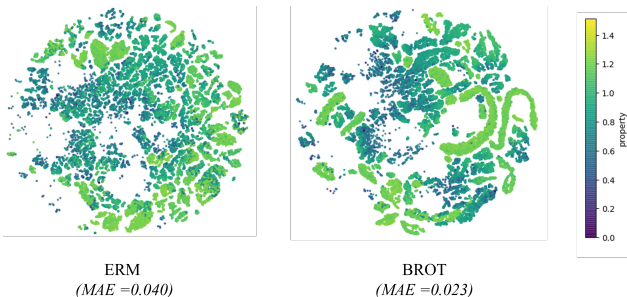


Figure 6. The t-SNE visualization of the UDA task in QM8. The brightness of green denotes the magnitude of molecular properties.

also discovered that a small  $\kappa$  ( $\kappa = 0.2$ ) benefits Semi-DA the most, while a extremely large  $\kappa$  ( $\kappa = 100$ ) may do great harm to the performance.

We envision feature distributions of ERM and BROT in QM8 by t-SNE projection (Van der Maaten & Hinton, 2008) in Figure 6. On the one hand, our approach realizes a lower MAE in the target domain, indicating its better capability of domain alignment. On the other hand, BROT succeeds at separating molecules of out-of-distribution (high) properties with molecules of in-distribution (low) properties. Thus, it can be widely applied in the biomedicine to seek drug-like molecules with desired outstanding properties, which may even never be seen in the source domain.

## 6. Conclusion

The adaptation across different domains guarantees the robustness of biomedical models and can greatly benefit the discovery of new drugs and materials. In this work, we represent a new optimal transport approach for biochemical regression domain adaptation problems with novel metrics and a posterior variance regularizer. To overcome the shortage of conventional metric and also mitigate the bias brought by computing mini-batches, a dynamic hierarchical triplet loss is introduced to help achieve more distinguishable decision boundaries and catch the global data distributions. We notably show it can reach state-of-the-art performances on challenging supervised and unsupervised tasks. We believe our studies will encourage more attention and shed light on



the biochemical domain adaptation applications.

## References

- Altschuler, J., Niles-Weed, J., and Rigollet, P. Near-linear time approximation algorithms for optimal transport via sinkhorn iteration. In Guyon, I., Luxburg, U. V., Bengio, S., Wallach, H., Fergus, R., Vishwanathan, S., and Garnett, R. (eds.), *Advances in Neural Information Processing Systems 30*, pp. 1964–1974. Curran Associates, Inc., 2017.
- Alvarez-Melis, D. and Fusi, N. Geometric dataset distances via optimal transport. *arXiv preprint arXiv:2002.02923*, 2020.
- Analytics, C. Web of science, 2017.
- Arjovsky, M., Bottou, L., Gulrajani, I., and Lopez-Paz, D. Invariant risk minimization. *arXiv preprint arXiv:1907.02893*, 2019.
- Blum, L. C. and Reymond, J.-L. 970 million druglike small molecules for virtual screening in the chemical universe database gdb-13. *Journal of the American Chemical Society*, 131(25):8732–8733, 2009.
- Bonnans, J. F. and Shapiro, A. Optimization problems with perturbations: A guided tour. *SIAM review*, 40(2):228–264, 1998.
- Chen, C., Ye, W., Zuo, Y., Zheng, C., and Ong, S. P. Graph networks as a universal machine learning framework for molecules and crystals. *Chemistry of Materials*, 31(9):3564–3572, 2019a.
- Chen, C., Zuo, Y., Ye, W., Li, X., and Ong, S. P. Learning properties of ordered and disordered materials from multi-fidelity data. *Nature Computational Science*, 1(1):46–53, 2021.
- Chen, G., Chen, P., Hsieh, C.-Y., Lee, C.-K., Liao, B., Liao, R., Liu, W., Qiu, J., Sun, Q., Tang, J., et al. Alchemy: A quantum chemistry dataset for benchmarking ai models. *arXiv preprint arXiv:1906.09427*, 2019b.
- Chung, Y. G., Haldoupis, E., Bucior, B. J., Haranczyk, M., Lee, S., Zhang, H., Vogiatzis, K. D., Milisavljevic, M., Ling, S., Camp, J. S., et al. Advances, updates, and analytics for the computation-ready, experimental metal-organic framework database: Core mof 2019. *Journal of Chemical & Engineering Data*, 64(12):5985–5998, 2019.
- Courty, N., Flamary, R., Tuia, D., and Rakotomamonjy, A. Optimal transport for domain adaptation. *IEEE transactions on pattern analysis and machine intelligence*, 39(9):1853–1865, 2016.
- Courty, N., Flamary, R., Habrard, A., and Rakotomamonjy, A. Joint distribution optimal transportation for domain adaptation. *arXiv preprint arXiv:1705.08848*, 2017.
- Creager, E., Jacobsen, J.-H., and Zemel, R. Exchanging lessons between algorithmic fairness and domain generalization. 2020.
- Cuturi, M. Sinkhorn distances: Lightspeed computation of optimal transport. *Advances in neural information processing systems*, 26:2292–2300, 2013.
- Damodaran, B. B., Kellenberger, B., Flamary, R., Tuia, D., and Courty, N. Deepjdot: Deep joint distribution optimal transport for unsupervised domain adaptation. In *Proceedings of the European Conference on Computer Vision (ECCV)*, pp. 447–463, 2018.
- Delaney, J. S. Esol: estimating aqueous solubility directly from molecular structure. *Journal of chemical information and computer sciences*, 44(3):1000–1005, 2004.
- Dhouib, S., Redko, I., Kerdoncuff, T., Emonet, R., and Sebban, M. A swiss army knife for minimax optimal transport. In *International Conference on Machine Learning*, pp. 2504–2513, 2020.
- Dou, Q., Coelho de Castro, D., Kamnitsas, K., and Glocker, B. Domain generalization via model-agnostic learning of semantic features. *Advances in Neural Information Processing Systems*, 32:6450–6461, 2019.
- Ertl, P., Rohde, B., and Selzer, P. Fast calculation of molecular polar surface area as a sum of fragment-based contributions and its application to the prediction of drug transport properties. *Journal of medicinal chemistry*, 43(20):3714–3717, 2000.
- Fatras, K., Séjourné, T., Flamary, R., and Courty, N. Unbalanced minibatch optimal transport; applications to domain adaptation. In *International Conference on Machine Learning*, pp. 3186–3197. PMLR, 2021a.
- Fatras, K., Zine, Y., Majewski, S., Flamary, R., Gribonval, R., and Courty, N. Minibatch optimal transport distances; analysis and applications. *arXiv preprint arXiv:2101.01792*, 2021b.
- Feinberg, E., Sheridan, R., Joshi, E., Pande, V., and Cheng, A. Step change improvement in admet prediction with potentialnet deep featurization. arxiv.org, 2019.
- Flamary, R., Courty, N., Gramfort, A., Alaya, M. Z., Boissunon, A., Chambon, S., Chapel, L., Corenflos, A., Fatras, K., Fournier, N., et al. Pot: Python optimal transport. *Journal of Machine Learning Research*, 22(78):1–8, 2021.

- Ganin, Y., Ustinova, E., Ajakan, H., Germain, P., Larochelle, H., Laviolette, F., Marchand, M., and Lempitsky, V. Domain-adversarial training of neural networks. *The journal of machine learning research*, 17(1):2096–2030, 2016.
- Gaulton, A., Bellis, L. J., Bento, A. P., Chambers, J., Davies, M., Hersey, A., Light, Y., McGlinchey, S., Michalovich, D., Al-Lazikani, B., et al. ChEMBL: a large-scale bioactivity database for drug discovery. *Nucleic acids research*, 40(D1):D1100–D1107, 2012.
- Ge, W. Deep metric learning with hierarchical triplet loss. In *Proceedings of the European Conference on Computer Vision (ECCV)*, pp. 269–285, 2018.
- Gómez-Bombarelli, R., Wei, J. N., Duvenaud, D., Hernández-Lobato, J. M., Sánchez-Lengeling, B., Sheberla, D., Aguilera-Iparraguirre, J., Hirzel, T. D., Adams, R. P., and Aspuru-Guzik, A. Automatic chemical design using a data-driven continuous representation of molecules. *ACS central science*, 4(2):268–276, 2018.
- Gong, B., Shi, Y., Sha, F., and Grauman, K. Geodesic flow kernel for unsupervised domain adaptation. In *2012 IEEE conference on computer vision and pattern recognition*, pp. 2066–2073. IEEE, 2012.
- Gopalan, R., Li, R., and Chellappa, R. Domain adaptation for object recognition: An unsupervised approach. In *2011 international conference on computer vision*, pp. 999–1006. IEEE, 2011.
- Groom, C. R., Bruno, I. J., Lightfoot, M. P., and Ward, S. C. The cambridge structural database. *Acta Crystallographica Section B: Structural Science, Crystal Engineering and Materials*, 72(2):171–179, 2016.
- Han, K., Lakshminarayanan, B., and Liu, J. Reliable graph neural networks for drug discovery under distributional shift. *arXiv preprint arXiv:2111.12951*, 2021.
- Hartigan, J. A. and Wong, M. A. Algorithm as 136: A k-means clustering algorithm. *Journal of the royal statistical society. series c (applied statistics)*, 28(1):100–108, 1979.
- Hendrycks, D. and Gimpel, K. A baseline for detecting misclassified and out-of-distribution examples in neural networks. *arXiv preprint arXiv:1610.02136*, 2016.
- Hsu, Y.-C., Shen, Y., Jin, H., and Kira, Z. Generalized odin: Detecting out-of-distribution image without learning from out-of-distribution data. In *Proceedings of the IEEE/CVF Conference on Computer Vision and Pattern Recognition*, pp. 10951–10960, 2020.
- Jhuo, I.-H., Liu, D., Lee, D., and Chang, S.-F. Robust visual domain adaptation with low-rank reconstruction. In *2012 IEEE conference on computer vision and pattern recognition*, pp. 2168–2175. IEEE, 2012.
- Jin, W., Barzilay, R., and Jaakkola, T. Enforcing predictive invariance across structured biomedical domains. *arXiv preprint arXiv:2006.03908*, 2020.
- Jumper, J., Evans, R., Pritzel, A., Green, T., Figurnoy, M., Ronneberger, O., Tunyasuvunakool, K., Bates, R., Žídek, A., Potapenko, A., et al. Highly accurate protein structure prediction with alphafold. *Nature*, 596(7873):583–589, 2021.
- Kerdoncuff, T., Emonet, R., and Sebban, M. Metric learning in optimal transport for domain adaptation. In *International Joint Conference on Artificial Intelligence*, 2021.
- Kingma, D. P. and Ba, J. Adam: A method for stochastic optimization. *arXiv preprint arXiv:1412.6980*, 2014.
- Krueger, D., Caballero, E., Jacobsen, J.-H., Zhang, A., Binas, J., Zhang, D., Le Priol, R., and Courville, A. Out-of-distribution generalization via risk extrapolation (rex). In *International Conference on Machine Learning*, pp. 5815–5826. PMLR, 2021.
- Kulis, B., Saenko, K., and Darrell, T. What you saw is not what you get: Domain adaptation using asymmetric kernel transforms. In *CVPR 2011*, pp. 1785–1792. IEEE, 2011.
- Kulis, B. et al. Metric learning: A survey. *Foundations and Trends® in Machine Learning*, 5(4):287–364, 2013.
- Landrum, G. Rdkit documentation. *Release*, 1(1-79):4, 2013.
- Langfelder, P., Zhang, B., and Horvath, S. Defining clusters from a hierarchical cluster tree: the dynamic tree cut package for r. *Bioinformatics*, 24(5):719–720, 2008.
- Le, T., Nguyen, T., Ho, N., Bui, H., and Phung, D. Lamda: Label matching deep domain adaptation. In *International Conference on Machine Learning*, pp. 6043–6054. PMLR, 2021.
- Leek, J. T., Scharpf, R. B., Bravo, H. C., Simcha, D., Langmead, B., Johnson, W. E., Geman, D., Baggerly, K., and Irizarry, R. A. Tackling the widespread and critical impact of batch effects in high-throughput data. *Nature Reviews Genetics*, 11(10):733–739, 2010.
- Li, B., Wang, Y., Zhang, S., Li, D., Keutzer, K., Darrell, T., and Zhao, H. Learning invariant representations and risks for semi-supervised domain adaptation. In *Proceedings of the IEEE/CVF Conference on Computer Vision and Pattern Recognition*, pp. 1104–1113, 2021.

- Li, D., Yang, Y., Song, Y.-Z., and Hospedales, T. M. Learning to generalize: Meta-learning for domain generalization. In *Thirty-Second AAAI Conference on Artificial Intelligence*, 2018.
- Li, M., Zhai, Y.-M., Luo, Y.-W., Ge, P.-F., and Ren, C.-X. Enhanced transport distance for unsupervised domain adaptation. In *Proceedings of the IEEE/CVF Conference on Computer Vision and Pattern Recognition*, pp. 13936–13944, 2020.
- Lin, J. Divergence measures based on the shannon entropy. *IEEE Transactions on Information theory*, 37(1):145–151, 1991.
- Long, M., Cao, Z., Wang, J., and Jordan, M. I. Conditional adversarial domain adaptation. *arXiv preprint arXiv:1705.10667*, 2017.
- Madani, A., McCann, B., Naik, N., Keskar, N. S., Anand, N., Eguchi, R. R., Huang, P.-S., and Socher, R. Progen: Language modeling for protein generation. *arXiv preprint arXiv:2004.03497*, 2020.
- Mobley, D. L. and Guthrie, J. P. Freesolv: a database of experimental and calculated hydration free energies, with input files. *Journal of computer-aided molecular design*, 28(7):711–720, 2014.
- Moore, A. K-means and hierarchical clustering, 2001.
- Nguyen, T., Le, T., Zhao, H., Tran, Q. H., Nguyen, T., and Phung, D. Most: Multi-source domain adaptation via optimal transport for student-teacher learning. In *Uncertainty in Artificial Intelligence*, pp. 225–235. PMLR, 2021.
- Paszke, A., Gross, S., Massa, F., Lerer, A., Bradbury, J., Chanan, G., Killeen, T., Lin, Z., Gimelshein, N., Antiga, L., et al. Pytorch: An imperative style, high-performance deep learning library. *Advances in neural information processing systems*, 32:8026–8037, 2019.
- Peyré, G., Cuturi, M., et al. Computational optimal transport: With applications to data science. *Foundations and Trends® in Machine Learning*, 11(5-6):355–607, 2019.
- Rakotomamonjy, A., Flamary, R., and Courty, N. Generalized conditional gradient: analysis of convergence and applications. *arXiv preprint arXiv:1510.06567*, 2015.
- Ramakrishnan, R., Dral, P. O., Rupp, M., and Von Lilienfeld, O. A. Quantum chemistry structures and properties of 134 kilo molecules. *Scientific data*, 1(1):1–7, 2014.
- Ramakrishnan, R., Hartmann, M., Tapavicza, E., and Von Lilienfeld, O. A. Electronic spectra from tddft and machine learning in chemical space. *The Journal of chemical physics*, 143(8):084111, 2015.
- Redko, I., Habrard, A., and Sebban, M. Theoretical analysis of domain adaptation with optimal transport. In *Joint European Conference on Machine Learning and Knowledge Discovery in Databases*, pp. 737–753. Springer, 2017.
- Sanchez-Lengeling, B. and Aspuru-Guzik, A. Inverse molecular design using machine learning: Generative models for matter engineering. *Science*, 361(6400):360–365, 2018.
- Seguy, V., Damodaran, B. B., Flamary, R., Courty, N., Rolet, A., and Blondel, M. Large-scale optimal transport and mapping estimation. *arXiv preprint arXiv:1711.02283*, 2017.
- Sun, B., Feng, J., and Saenko, K. Correlation alignment for unsupervised domain adaptation. In *Domain Adaptation in Computer Vision Applications*, pp. 153–171. Springer, 2017.
- Townshend, R. J., Vögele, M., Suriana, P., Derry, A., Powers, A., Laloudakis, Y., Balachandar, S., Jing, B., Anderson, B., Eismann, S., et al. Atom3d: Tasks on molecules in three dimensions. *arXiv preprint arXiv:2012.04035*, 2020.
- Tsubaki, M. and Mizoguchi, T. Quantum deep field: Data-driven wave function, electron density generation, and atomization energy prediction and extrapolation with machine learning. *Physical Review Letters*, 125(20):206401, 2020.
- Van der Maaten, L. and Hinton, G. Visualizing data using t-sne. *Journal of machine learning research*, 9(11), 2008.
- Vaswani, A., Shazeer, N., Parmar, N., Uszkoreit, J., Jones, L., Gomez, A. N., Kaiser, Ł., and Polosukhin, I. Attention is all you need. In *Advances in neural information processing systems*, pp. 5998–6008, 2017.
- Wang, R., Fang, X., Lu, Y., Yang, C.-Y., and Wang, S. The pdbname database: methodologies and updates. *Journal of medicinal chemistry*, 48(12):4111–4119, 2005.
- Weed, J. and Bach, F. Sharp asymptotic and finite-sample rates of convergence of empirical measures in wasserstein distance. *Bernoulli*, 2019.
- Wu, F., Zhang, Q., Radev, D., Cui, J., Zhang, W., Xing, H., Zhang, N., and Chen, H. 3d-transformer: Molecular representation with transformer in 3d space. *arXiv preprint arXiv:2110.01191*, 2021.
- Wu, Z., Ramsundar, B., Feinberg, E. N., Gomes, J., Geniesse, C., Pappu, A. S., Leswing, K., and Pande, V. Moleculenet: a benchmark for molecular machine learning. *Chemical science*, 9(2):513–530, 2018.

- Yan, Y., Li, W., Wu, H., Min, H., Tan, M., and Wu, Q. Semi-supervised optimal transport for heterogeneous domain adaptation. In *IJCAI*, volume 7, pp. 2969–2975, 2018.
- Yang, J., Zhou, K., Li, Y., and Liu, Z. Generalized out-of-distribution detection: A survey. *arXiv preprint arXiv:2110.11334*, 2021.
- Ye, H., Xie, C., Cai, T., Li, R., Li, Z., and Wang, L. Towards a theoretical framework of out-of-distribution generalization. *arXiv preprint arXiv:2106.04496*, 2021.
- Zhang, C., Cai, Y., Lin, G., and Shen, C. Deepemd: Few-shot image classification with differentiable earth mover’s distance and structured classifiers. In *Proceedings of the IEEE/CVF conference on computer vision and pattern recognition*, pp. 12203–12213, 2020.
- Zhang, Z., Liu, Q., Wang, H., Lu, C., and Lee, C.-K. Motif-based graph self-supervised learning for molecular property prediction. *Advances in Neural Information Processing Systems*, 34, 2021.
- Zhou, F., Jiang, Z., Shui, C., Wang, B., and Chaib-draa, B. Domain generalization with optimal transport and metric learning. *arXiv preprint arXiv:2007.10573*, 2020.

## A. Preliminary (Continued)

### A.1. Theoretical Assumptions

With the hypothesis that  $\mathcal{P}^s$  and  $\mathcal{P}^t$  exist, then at least one of the two following assumptions is generally recognized by most DA approaches (Courty et al., 2016), and they are suitable for our biochemical DA problems as well:

**Property imbalance.** Property distributions are different in the two domains as  $\mathbb{P}_s(\mathbf{y}^s) \neq \mathbb{P}_t(\mathbf{y}^t)$ , but the conditional distributions of molecules with respect to the properties are the same as  $\mathbb{P}_s(\mathbf{x}^s|\mathbf{y}^s) = \mathbb{P}_t(\mathbf{x}^t|\mathbf{y}^t)$ .

**Covariate shift.** Conditional distributions of the properties with respect to molecules are equal or equivalent as  $\mathbb{P}_s(\mathbf{y}^s|\mathbf{x}^s) = \mathbb{P}_t(\mathbf{y}^t|\mathbf{x}^t)$ . Nevertheless, data distributions in two domains are assumed to be different  $\mathbb{P}_s(\mathbf{x}^s) \neq \mathbb{P}_t(\mathbf{x}^t)$ .

### A.2. Variation and Informativeness

As analyzed before, target properties can explicitly determine SS but not NS in biomedical data, since molecules of different categories can share overlapped property distributions. Therefore, we combine molecular representations  $f(\mathcal{X})$  and properties  $\mathcal{Y}$  together to a joint distribution  $\mathbb{P}(f(\mathcal{X}), \mathcal{Y})$ , and use it to describe the connection between  $\mathcal{E}^s$  and  $\mathcal{E}^t$ . Then given a symmetric metric  $\rho$  to evaluate the distance between two distributions, the following Equations measure the variation and informativeness of the feature extractor  $f$  across  $\mathcal{E}^s$  and  $\mathcal{E}^t$  (Ye et al., 2021):

$$\mathcal{V}_\rho(f, \mathcal{E}^s, \mathcal{E}^t) = \max_{\mathbf{y}^s \in \mathcal{Y}^s, \mathbf{y}^t \in \mathcal{Y}^t} \sup_{\substack{s \in \mathcal{E}^s \\ t \in \mathcal{E}^t}} \rho(\mathbb{P}(f(\mathbf{x}^s)|\mathbf{y}^s), \mathbb{P}(f(\mathbf{x}^t)|\mathbf{y}^t)) \quad (16)$$

$$\mathcal{I}_\rho(f, \mathcal{E}^s, \mathcal{E}^t) = \min_{\substack{\mathbf{y}^s \neq \mathbf{y}^t \\ \mathbf{y}^s \in \mathcal{Y}^s, \mathbf{y}^t \in \mathcal{Y}^t}} \inf_{\substack{s \in \mathcal{E}^s \\ t \in \mathcal{E}^t}} \rho(\mathbb{P}(f(\mathbf{x}^s)|\mathbf{y}^s), \mathbb{P}(f(\mathbf{x}^t)|\mathbf{y}^t)) \quad (17)$$

Here,  $\mathcal{V}_\rho(f, \mathcal{E}^s, \mathcal{E}^t)$  measures the stability of  $f$  over two given domain sets, and  $\mathcal{I}_\rho(f, \mathcal{E}^s, \mathcal{E}^t)$  captures the eligibility of  $R$  to distinguish properties of different values. Since DA is always associated with a low  $\mathcal{V}_\rho(f, \mathcal{E}^s, \mathcal{E}^t)$  and a high  $\mathcal{I}_\rho(f, \mathcal{E}^s, \mathcal{E}^t)$ , we aim to decrease  $\mathcal{V}_\rho(f, \mathcal{E}^s, \mathcal{E}^t)$  and increase  $\mathcal{I}_\rho(f, \mathcal{E}^s, \mathcal{E}^t)$  as more as possible.

## B. JS-distance for Semi-DA

### B.1. Instance Study

There we implement a case study to better understand drawbacks of the simple additive metric and the advantage of our proposed JS-distance metric. There are two source points  $(\mathbf{x}_1^s, \mathbf{y}_1^s)$ ,  $(\mathbf{x}_2^s, \mathbf{y}_2^s)$  and two target points  $(\mathbf{x}_1^t, \mathbf{y}_1^t)$ ,  $(\mathbf{x}_2^t, \mathbf{y}_2^t)$ , and we consider a Monge problem with  $T_{ij} \in \{0, 1\}, \forall i, j$ . The distance between each source-target pair is marked along the dotted edges (see Figure 8).

For additive distance metric with  $\epsilon = 1$ , since  $d_{\mathcal{Z}}^f((\mathbf{x}_1^s, \mathbf{y}_1^s), (\mathbf{x}_1^t, \mathbf{y}_1^t)) + d_{\mathcal{Z}}^f((\mathbf{x}_2^s, \mathbf{y}_2^s), (\mathbf{x}_2^t, \mathbf{y}_2^t)) = 15 < d_{\mathcal{Z}}^f((\mathbf{x}_1^s, \mathbf{y}_1^s), (\mathbf{x}_2^t, \mathbf{y}_2^t)) + d_{\mathcal{Z}}^f((\mathbf{x}_2^s, \mathbf{y}_2^s), (\mathbf{x}_1^t, \mathbf{y}_1^t)) = 16$ . Its transport plan is to match  $(\mathbf{x}_1^s, \mathbf{y}_1^s)$  with  $(\mathbf{x}_1^t, \mathbf{y}_1^t)$  and match  $(\mathbf{x}_2^s, \mathbf{y}_2^s)$  with  $(\mathbf{x}_2^t, \mathbf{y}_2^t)$ . However, this matching is not optimal, and violates the basic principle that every source-target pair

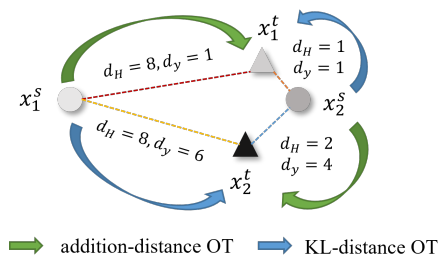


Figure 7. An instance study of different metrics in Semi-DA, where distances of each source-target pair in  $\mathcal{H}$  and  $\mathcal{Y}$  are given along dotted lines and the darkness represents the magnitude of properties. The arrows denote the matching of source-target pairs under different distance metrics.

with close properties tend to share analogous features. Properties of  $\mathbf{x}_1^s$  and  $\mathbf{x}_1^t$  are similar but they are distant to each other in the feature space  $\mathcal{H}$ .

On the other hand, our JS-distance takes fully considerations of the relative size between  $d_{\mathcal{H}}$  and  $d_{\mathcal{Y}}$ . Assume  $\zeta = 0$ , then  $d_{\mathcal{Z}}^f((\mathbf{x}_1^s, y_1^s), (\mathbf{x}_1^t, y_1^t)) + d_{\mathcal{Z}}^f((\mathbf{x}_2^s, y_2^s), (\mathbf{x}_2^t, y_2^t)) = 2.083 + 0.480 \cdot \kappa$ , while  $d_{\mathcal{Z}}^f((\mathbf{x}_1^s, y_1^s), (\mathbf{x}_2^t, y_2^t)) + d_{\mathcal{Z}}^f((\mathbf{x}_2^s, y_2^s), (\mathbf{x}_1^t, y_1^t)) = 2.291 + 0.036 \cdot \kappa$ . Once we select a  $\kappa \geq 0.46$ , our transport plan is able to distinguish the divergence of  $d_{\mathcal{H}}$  and  $d_{\mathcal{Y}}$ . Then it leads to the ideal plan that moves  $(\mathbf{x}_1^s, y_1^s)$  to  $(\mathbf{x}_2^t, y_2^t)$ , and  $(\mathbf{x}_2^s, y_2^s)$  to  $(\mathbf{x}_1^t, y_1^t)$  separately. This instance analysis strongly supports our statement that JS-distance metric outweighs additive distance metric in the sense that our JS-distance will never associate samples with similar properties but completely different features or vice reverse.

## B.2. Influence of $\kappa$

Since  $\kappa$  is a hyper-parameter in Equation 5, We visualize the cost functions of  $d_{\mathcal{Z}}^f$  under different  $\kappa$  to explore its influence. More empirical comparisons of different  $\kappa$  are in Appendix D.4.

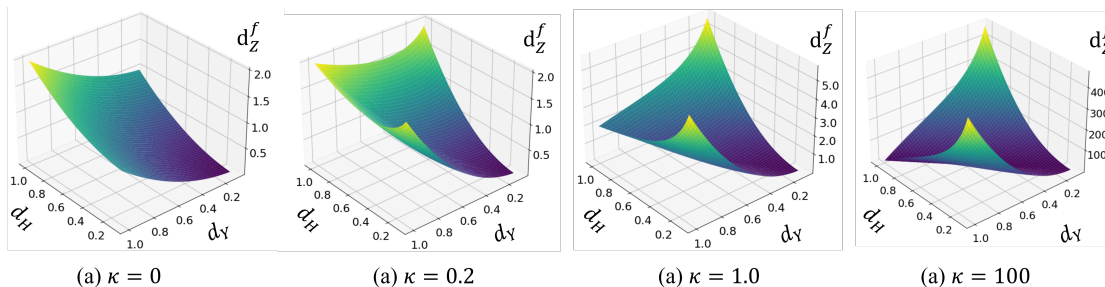


Figure 8. Cost functions with different  $\kappa$ . The  $x$ - and  $y$ -axis correspond to the distances in  $\mathcal{H}$  and  $\mathcal{Y}$ , and the darkness of color reflects the magnitude of  $d_{\mathcal{Z}}^f$ .

## C. Posterior Variance Regularization

### C.1. The posterior variance regularizer is concave in $\mathbf{T}$

In this part we show that the posterior variance regularizer is concave *wrt.* the coupling  $\mathbf{T}$ , allowing to solve the underlying optimization problem as a DC program.

**Proposition C.1.** *Let  $\mathbf{T} \in \Pi(\mathcal{B}^s, \mathcal{B}^t)$  be a coupling between two batches of size  $b$ . Then  $\Omega_{\mathbf{p}}^{\mathcal{Y}^s}(\mathbf{T})$  is concave in  $\mathbf{T}$ .*

*Proof.* This directly follows the fact that the variance is concave in that the variance  $\text{var}_{\mathbf{p}}(Y)$  of a random variable  $Y$  taking values in  $\{y_0, \dots, y_{b-1}\}$  with probability  $\mathbf{p} \in \Delta^{b-1}$  (the probability simplex) is concave in  $\mathbf{p}$ . Knowing that  $\text{var}_{\mathbf{p}}(Y) = \mathbb{E}_{\mathbf{p}}[Y^2] - \mathbb{E}_{\mathbf{p}}[Y]^2$ , we have that, for any  $\lambda \in [0, 1]$  and  $\mathbf{q} \in \Delta^{b-1}$ :

$$\mathbb{E}_{\lambda\mathbf{p}+(1-\lambda)\mathbf{q}}[Y^2] = \lambda\mathbb{E}_{\mathbf{p}}[Y^2] + (1-\lambda)\mathbb{E}_{\mathbf{q}}[Y^2]. \quad (18)$$

We then have that:

$$\lambda\mathbb{E}_{\mathbf{p}}[Y]^2 + (1-\lambda)\mathbb{E}_{\mathbf{q}}[Y]^2 \geq (\lambda\mathbb{E}_{\mathbf{p}}[Y] + (1-\lambda)\mathbb{E}_{\mathbf{q}}[Y])^2 \quad (19)$$

$$= \mathbb{E}_{\lambda\mathbf{p}+(1-\lambda)\mathbf{q}}[Y]^2, \quad (20)$$

where the first inequality is obtained by Jensen inequality. Subsequently, we have that

$$\text{var}_{\lambda\mathbf{p}+(1-\lambda)\mathbf{q}}(Y) = \mathbb{E}_{\lambda\mathbf{p}+(1-\lambda)\mathbf{q}}[Y^2] - \mathbb{E}_{\lambda\mathbf{p}+(1-\lambda)\mathbf{q}}[Y]^2 \quad (21)$$

$$\geq \lambda\text{var}_{\mathbf{p}}(Y) + (1-\lambda)\text{var}_{\mathbf{q}}(Y), \quad (22)$$

which is sufficient to say that the variance  $\text{var}_{\mathbf{p}}$  is concave *wrt.*  $\mathbf{p}$ . Finally, the concavity of  $\Omega_{\mathbf{p}}^{\mathcal{Y}^s}(\mathbf{T}) = \sum_j \text{var}_{\mathbf{t}_j}(Y_j)$  is established as being a sum of concave functions.  $\square$

## C.2. Gradient of posterior variance regularizer and optimization

In order to solve Problem 9, that we need to compute the solution of a regularized optimal problem, conducted over batches of data, that we recall here:

$$\mathbf{T}^* = \operatorname{argmin}_{\mathbf{T} \in \Pi(\mathcal{B}^s, \mathcal{B}^t)} \langle \mathbf{T}, \mathbf{D}_{\mathcal{Z}}^f \rangle + \lambda_1 \Omega_e(\mathbf{T}) + \lambda_2 \Omega_p^{y^s}(\mathbf{T}), \quad (23)$$

We use a generalized conditional gradient (Rakotomamonjy et al., 2015) optimization method, that relies on a local linearization of a sub-part of the problem. In a nutshell (see (Courty et al., 2016) for a detailed description of the procedure), we iterate over several resolution of the following entropy regularized problem:

$$\mathbf{T}_{k+1}^* = \operatorname{argmin}_{\mathbf{T} \in \Pi(\mathcal{B}^s, \mathcal{B}^t)} \langle \mathbf{T}, \mathbf{D}_{\mathcal{Z}}^f + \lambda_2 \nabla_{\mathbf{T}_k} \Omega_p^{y^s}(\mathbf{T}_k) \rangle + \lambda_1 \Omega_e(\mathbf{T}), \quad (24)$$

With  $k$  denoting the iteration.

We provide here the derivation of the gradient of  $\Omega_p^{y^s}(\mathbf{T})$  wrt.  $\mathbf{T}$ . We first recall the expression of this regularizer:

$$\Omega_p^{y^s}(\mathbf{T}) = \sum_{j=1}^b \operatorname{var}_{\mathbf{t}_j}(Y_j) \quad (25)$$

$$= b \sum_{j=1}^b \sum_{i=1}^b T_{ij} \left( y_i^s - \sum_{l=1}^b b T_{lj} \cdot y_l^s \right)^2 \quad (26)$$

$$= \sum_{j=1}^b \sum_{i=1}^b b T_{ij} \cdot y_i^{s2} - \sum_{j=1}^b \left( \sum_{i=1}^b b T_{ij} \cdot y_i^s \right)^2 \quad (27)$$

Thus, its gradient follows simply as:

$$\nabla_{\mathbf{T}} \Omega_p^{y^s}(\mathbf{T}) = \left[ b y_i^{s2} - 2 b^2 y_i^s \sum_{l=1}^b T_{lj} \cdot y_l^s \right]_{i \in [b], j \in [b]} \quad (28)$$

$$= b \left( \mathbf{y}^{s2} \mathbf{1}_b^T - 2 b \mathbf{y}^s (\mathbf{y}^{sT} \mathbf{T})^T \right) \quad (29)$$

where  $\mathbf{1}_b$  is a  $b$ -dimension vector composed of ones. In practice, we use the implementation of this method provided by the POT (Flamary et al., 2021) library.

## D. Experiment

In this section, we provide details of datasets, the model architecture, baseline methods and the training procedure for the experiments. All experiments are implemented using Pytorch (Paszke et al., 2019) and run on A40 GPUs with 45.63G memory.

### D.1. Dataset

The statistical data of eight datasets used in the experiments are enumerated in Table D.1, including the number of tasks, the number of molecules and atom classes, the minimum and maximum number of atoms, and their evaluation metrics. Though QM8 possesses 12 tasks, we only take the target 'E1-CC2' into consideration. Since Molformer takes 3D coordinates as input, we use RDKit (Landrum, 2013) to procure 3D conformations of each molecule from SMILES for ESOL, FreeSolv, and Lipophilicity.

### D.2. Model Architecture and Baselines

Molformer (Wu et al., 2021) is adopted for feature extraction  $f$ . It has 2 layer and 4 multi-scale attention heads with local scales of 0.6 and 1.5 Å. The dropout rate is set as 0.1 across all layers. The input embedding size is 512 and the hidden size for feed-forward neural networks is 2048. There we abandon the extraction of motifs and only use the atom-level molecular graphs rather than heterogeneous molecular graphs for simplicity. The top regressor  $h$  is a two-layer MLP. The discriminators in DANN and CADN all use a two-layer MLP.

Table 4. Key statistics of datasets from three different biochemical fields.

Category	Dataset	Tasks	Task Type	Molecules	Atom Class	Min. Atoms	Max. Atoms	Metric
Quantum Chemistry	QM7	1	regression	7,160	5	4	23	MAE
	QM8	12	regression	21,786	5	3	26	MAE
	QM9	12	regression	133,885	5	3	28	MAE
Physical Chemistry	ESOL	1	regression	1,128	9	1	55	RMSE
	FreeSolv	1	regression	643	9	1	24	RMSE
	Lipophilicity	1	regression	4,200	12	7	115	RMSE
Material Science	CoRE-MOF	6	regression	10,066	77	10	10,560	RMSE
	Exp-MOF	1	regression	113	25	11	3,594	RMSE

For JDOT, instead of minimizing the distance between the input  $\mathbf{x}_i^s$  and  $\mathbf{x}_j^t$ , we seek to optimize the distance between representations of samples, because it is hard to immediately measure the distance between two molecules. The extractor  $f$  is to be learned according to the following optimization problem:

$$\min_{f, \pi \in \Pi(\mathcal{P}^s, \mathcal{P}^t)} \sum_{i,j} \pi_{i,j} (d_{\mathcal{H}}(f(\mathbf{x}_i^s), f(\mathbf{x}_j^t)) + \epsilon' \mathcal{L}(y_i^s, f(\mathbf{x}_j^t))) + \lambda \Omega(f) \quad (30)$$

where  $\epsilon'$  is the balance weight, and  $L$  is the metric in  $\mathcal{H}$  analogical to  $d_y$  but is continuous and differentiable *wrt.* its second variable. We also add the cross entropy regularization and employ the Sinkhorn algorithm to optimize this Equation.

### D.3. Training Details and hyperparameter

For QM7, QM8, ESOL, FreeSolv, and Lipophilicity, we use a training batch size of 1024 and the maximum epochs is 100. For QM9, we choose a batch size of 4096 and the maximum epochs is 200. For CORE-MOF and Exp-MOF, we adopt a training batch size of 64, and all crystals are truncated to a maximum length of 512. An early stopping mechanism is utilized once the training loss no longer decreases for 30 epochs. An Adam (Kingma & Ba, 2014) optimizer is used and a ReduceLRonPlateau scheduler is enforced to adjust it with a factor of 0.6 and a patience of 10. We apply no weight decay there. The initial learning rate is set as  $10^{-4}$ . For OT optimization problems, we use POT (Flamary et al., 2021), an open and efficient Python library to solve them. For t-SNE visualization, we run 2K iterations using the Scikit-learn package.

We follow the protocol of Courty et al. (2016) to tune the hyperparameter of our model and baselines throughout grid search. To be precise, they are tuned based on the validation dataset, and the adaptation error is then evaluated on the test set, with the best selected hyperparameter. This strategy normally prevents overfitting in the test set. The range of those hyperparameter are shown in Table 5.

Table 5. The training hyperparameter.

Hyper-parameter	Description	Range
bs	The input batch size.	[32, 64, 128, 512, 1024, 2048, 4096]
lr	The initial learning rate of ReduceLRonPlateau learning rate scheduler.	[1e-4, 1e-5]
min_lr	The minimum learning rate of ReduceLRonPlateau learning rate scheduler.	[1e-7, 5e-7]
n_clusters	The number of the finest-grained (initial) clusters.	[8, 16, 32, 64, 128, 512]
zeta	The additional term to prevent the zero division error.	[1e-3, 5e-3, 1e-2]
epsilon	The weight to control distance in the property space in JS-distance.	[0.1, 1, 5, 10]
kappa	The weight for the JS term in distance metric for Semi-DA.	[0.05, 0.1, 0.2, 0.3]
mu	The constant parameter in the hierarchical violate margin.	[1e-4, 1e-3]
ot_weight	The weight for OT loss.	[1e5, 1e6, 1e7, 1e8, 1e9, 1e10, 1e11, 1e12]
triplet_loss	The weight for triplet loss.	[1e-2, 1e-1, 1, 1e, 1e2, 1e3]
reg1	The entropic regularization term in OT.	[1e-2, 1e-1, 1, 1e, 1e2]
reg2	The posterior variance regularization term in OT.	[1e-2, 1e-1, 1, 1e, 1e2]
meta_val_beta	The strength of the meta validation loss for the baseline MLDG method.	[1e-1, 2e-1, 5e-1]



#### D.4. Additional Ablation Study

We re-exam the effectiveness of our proposed JS-distance metric over additive distance metric for Semi-DA tasks. The empirical results in Table 6 demonstrate that JS-distance outperform additive distance in the biochemical Semi-DA problems with generally higher Pearson and Spearman correlations and a lower RMSE.

Table 6. Comparison of RMSE,  $R_p$  and  $R_s$  on Exp-MOF with 25% and 50% labeled target data.

Method	25% Labeled Target			50% Labeled Target		
	RMSE	$R_p$	$R_s$	RMSE	$R_p$	$R_s$
Additive Distance	<u>21.70</u>	<b>0.588</b>	<u>0.580</u>	<u>19.86</u>	0.588	<u>0.614</u>
JS-distance ( $\kappa = 0.2$ )	<b>20.45</b>	<u>0.552</u>	<b>0.617</b>	<b>19.42</b>	<b>0.659</b>	<b>0.710</b>
JS-distance ( $\kappa = 1.0$ )	25.12	0.523	0.554	20.70	0.586	0.607
JS-distance ( $\kappa = 100$ )	29.91	0.478	0.502	24.15	0.477	0.553